

# Promoting Effects of Na and Fe Impurities on the Catalytic Activity of CaO in the Reduction of NO by CO and H<sub>2</sub>

Filip Acke\* and Itai Panas

Department of Inorganic Chemistry, Chalmers University of Technology and Göteborg University, S-412 96 Göteborg, Sweden

Received: January 29, 1998; In Final Form: April 16, 1998

The heterogeneous reduction of NO by H<sub>2</sub> and CO over different CaO materials is investigated. The dependence of the specific NO reduction rate on the impurity content is demonstrated for both reducing species. The roles of two specific impurities, i.e., Na and Fe, as well as their combined effect are investigated. The apparent activation energies for the NO + CO and NO + H<sub>2</sub> reactions are determined for three different calcium oxides. Values between 26 and 28 kcal/mol are obtained. The influence of impurity content is found in the preexponential factor of the Arrhenius equation. A reaction mechanism based on a rate-determining surface-oxygen-abstraction step is suggested. This mechanistic understanding is explored to compare the activities of other alkaline-earth oxides. Particularly, a linear correlation between the apparent activation energy and the lattice parameter is observed.

## I. Introduction

Emissions of nitrogen oxides are a threat to the environment. The use of catalytic materials to reduce NO<sub>x</sub> is one of the techniques that is available to efficiently control these emissions. Noble metals are an example of thoroughly investigated materials that show a high activity toward NO<sub>x</sub> reduction. To regenerate the active surface, the presence of reducing agents, e.g., CO, H<sub>2</sub>, and hydrocarbons, has been shown to be necessary.<sup>1</sup> Model catalysts in the nano- and microscale<sup>2</sup> and single crystals<sup>3,4</sup> are used in the search for a mechanistic understanding of the reduction of NO. Transition-metal oxides are another class of materials that have been shown to be catalytically active for these reactions.<sup>5</sup> Perovskites were especially believed to be promising representatives,<sup>6,7</sup> for which lattice oxygens were suggested to participate in the reaction.<sup>8</sup>

The participation of lattice oxygens has also been discussed for the oxidative coupling of methane over alkali-metal-doped alkaline-earth oxides.<sup>9,10</sup> In a previous work, this was shown to even hold for the NO reduction over CaO.<sup>11</sup> The activity of CaO might be surprising because the solid has a filled valence band and a bulk band gap of about 7 eV.<sup>12</sup> Two models were suggested to explain the involvement of promoters on the participation of lattice oxygens in the reaction mechanism, i.e., a semiconductor model<sup>10</sup> and a model based on F-type centers.<sup>9</sup> In case of the former, alkali-metal ions are introduced into an alkaline-earth oxide to provide electron acceptors in the band gap, while in the latter they are introduced to stabilize F centers. A mechanism was suggested based on an oxygen-abstraction step and a reoxidation of the surface.<sup>9,10</sup> The activation energy for the oxygen-abstraction step using CO as the reducing agent is 25 kcal/mol. The reoxidation of the surface, using NO as the oxidant, displays a 10 kcal/mol upper limit for the apparent activation energy.<sup>11</sup>

A dependence on the amount of dopant of the catalytic activity for NO reduction with methane was shown by Zhang

et al.<sup>13</sup> for Li-promoted MgO substrates. An initial increase of the specific activity was observed with Li doping. The importance of the impurity level as well as the chemical surrounding of the impurity has been discussed for iron in quartz.<sup>14</sup> It was shown that Fe as an impurity is not catalytically active when iron is incorporated in a well-defined crystal structure (illite). To be active, the electronic structure had to be affected or crystal defects produced.

In this article, a comparison of the catalytic activities will be presented for different CaO materials toward the reduction of NO with CO and H<sub>2</sub>. It will be shown that the different impurities do not significantly affect the apparent activation energy for the NO reduction with H<sub>2</sub> but that the importance of the impurities has to be found in the preexponential factor of the Arrhenius equation, i.e., the amount of defects produced. It will be shown that the results for H<sub>2</sub> as a reducing agent agree with those of CO after correction for CO<sub>2</sub> poisoning. The effect of Na and Fe impurities on the reduction of NO with H<sub>2</sub> will be carefully investigated by the preparation of CaO powders containing equimolecular amounts of Na, Fe, and Na + Fe.

## II. Experimental Section

**II.1. Preparation of the CaO Powders.** The tested powders are listed in Table 1. They can be divided into three groups: pure, as received, and promoted CaO powders. The purification step, for the *pure materials*, is based on the low solubility of CaCO<sub>3</sub> in water. A CaO powder was first dissolved in milli-Q water, and the dissolved Ca<sup>2+</sup> ions were subsequently precipitated as a carbonate by bubbling through CO<sub>2</sub>. This solution is then filtered, and the precipitate is heat-treated at 950 °C for 2.5 h in an oxygen flow, resulting in the purified CaO. Other carbonates such as Na<sub>2</sub>CO<sub>3</sub> are much more soluble and will stay in solution.

Three different types of *promoted CaO materials* were prepared by doping with Na, Fe, and Na + Fe. The promoters were added as sodium carbonate and/or iron acetate to a calcium acetate solution. By evaporation of the water, a promoted

\* Corresponding author. Telephone: +46 (0)31 772 28 86, Fax: +46 (0) 31 772 28 53. E-mail: filip@inoc.chalmers.se.

**TABLE 1: (a) Iron and Sodium Contents, and Specific Surface Areas of the Investigated CaO Materials and (B) Added Amounts of Iron and Sodium (Both as wt % and mol %), as Well as Specific Surface Areas of the CaO Materials Prepared for the Detailed Analysis of the Na, Fe, and Na + Fe Contents on the Catalytic Activities of CaO**

Section A					
material		AAS, wt %		BET, (m <sup>2</sup> /g)	
		Fe	Na		
CaO/Fisher Scientific		0.052	0.010	2.3	
CaO/Ph DAB pieces	as received	0.029	0.011	1.6	
CaO/Ph DAB pieces	purified	0.004	0.004	9.2	
CaO from Ca(OH) <sub>2</sub> /Merck	as received	0.042	0.014	4.9	
CaO from Ca(OH) <sub>2</sub> /Merck	purified	0.004	0.003	14.4	
CaO from Ca-acetate Fisher Scientific		0.003	0.005	11.6	
Na doped CaO	label 1	0.003	0.200	0.8	
	label 2	0.003	0.508	0.6	
	label 3	0.003	0.470	0.4	
	label 4	0.008	0.268	0.6	
Section B					
material	added amount, wt %		added amount, mol %		BET, m <sup>2</sup> /g
	Fe	Na	Fe	Na	
Na 0.001	0	0.05	0	$1.24 \times 10^{-3}$	7.3
Na 0.004	0	0.15	0	$3.72 \times 10^{-3}$	3.7
Na 0.007	0	0.30	0	$7.44 \times 10^{-3}$	2.7
Fe 0.001	0.12	0	$1.24 \times 10^{-3}$	0	8.1
Fe 0.004	0.37	0	$3.72 \times 10^{-3}$	0	7.4
Fe 0.007	0.74	0	$7.44 \times 10^{-3}$	0	7.2
Na + Fe 0.001	0.12	0.05	$1.24 \times 10^{-3}$	$1.24 \times 10^{-3}$	4.6
Na + Fe 0.004	0.37	0.15	$3.72 \times 10^{-3}$	$3.72 \times 10^{-3}$	3.1
Na + Fe 0.008	0.74	0.30	$7.44 \times 10^{-3}$	$7.44 \times 10^{-3}$	1.7

calcium acetate was obtained. Calcination of the acetate was done in an oxygen flow at 950 °C for 2.5 h. To make clear that the change in catalytic activity was due to the addition of dopants and not to the treatment, a blank was prepared. The Na-promoted materials can be divided in two groups, i.e., the ones labeled 1–4 (Table 1A) and the ones labeled 0.001, 0.004, and 0.007 (Table 1B). The latter are part of a group of materials that were prepared to clarify the possible synergistic effects between Na and Fe impurities. These materials contained equimolecular amounts of Na, Fe, and Na + Fe.

**II.2. Specific Surface Area.** The specific surface areas of the investigated materials were determined by nitrogen adsorption–desorption with a Digisorb 2600 instrument (Micrometrics). The BET surface area determinations were based on five experiments at relative pressures of nitrogen in the range of 0.05–0.21. The used cross-sectional area of the nitrogen adsorbate was 0.162 nm<sup>2</sup>.

**II.3. Experimental Setups and Testing Procedures.** The first set of experiments investigate the catalytic activity of the CaO materials listed in Table 1A toward the reduction of NO with CO and H<sub>2</sub>. The experiments were performed in a fixed-bed reactor. One-half gram of catalytic material was mixed with 5 g of quartz sand (quartz fine granular, pro analysi from Merck). The sample was placed on a sintered quartz filter in a quartz reactor with a 28-mm inner diameter and a length of 1000 mm. The gas flow, measured at ambient temperature and pressure, was 580 mL/min. This results in residence times for the different tested materials of between 50 and 63 ms at 800 °C. Gas mixtures of 1000 ppm NO and 1000 ppm CO or H<sub>2</sub> in Ar were used for all samples. These gas mixtures simplify the solution of the mass balance significantly. The temperature was measured with a Pt–13% Rh/Pt thermocouple, shielded with a quartz tube and situated about 0.5 cm above the bed. The temperature was kept between 799 and 801 °C by using a Eurotherm thermoregulator. A quadrupole mass spectrometer, Type QMG 421(Balzars), was employed to detect the decrease in NO concentration between a gas flow bypassing the reactor

and the gas flow passing through the reactor. No mass-transport problems and no catalytic activity other than the one due to the added material were observed.

Measurements of the kinetic parameters were done for three of the powders listed in Table 1A in a fixed-bed reactor connected to a photoacoustic Fourier transform infrared (FTIR) gas analyzer from Brüel and Kjaer (one of each group, i.e., a pure, an as-received, and a Na-doped). One-half gram of the tested catalytic materials was mixed with different amounts of quartz sand (4, 6, and 10 g), changing the residence times in the range of 33–176 ms. The mixtures were placed on a sintered quartz filter. A quartz reactor with an inner diameter of 22 mm and a length of 500 mm was used for the kinetic study. The reactor had an asymmetric construction to avoid heating of the upper metal fitting and the vacuum-tight Viton O-ring. The temperature was measured with a nickel–chrome thermocouple positioned 0.5 cm below the sintered quartz filter and 3 mm below the outlet of the reactor. The positioning of the thermocouple in this way avoids any interference on the results. The bed materials were exposed to different gas mixtures: 862 ppm NO/918 ppm CO or H<sub>2</sub>, 844 ppm NO/424 ppm CO or H<sub>2</sub>, and 635 ppm NO/890 ppm CO or H<sub>2</sub>. The first gas mixture was tested at two different flows, 693.4 and 433.5 mL/min, while the other two mixtures were only tested using a flow of 525 mL/min. All flows refer to room temperature and atmospheric pressure. The results were checked for influences of mass transport and interference of metal parts in the reactor.

The latter experimental setup was also used to investigate the possible synergistic effects between Na and Fe impurities on the catalytic activity of doped CaO materials. A reaction mixture of 1000 ppm H<sub>2</sub> and 700 ppm NO was used to determine the NO reaction rate for the materials listed in Table 1B, using a flow of 450 mL/min at 800 °C. H<sub>2</sub> was used as the reducing agent in order to avoid CO<sub>2</sub> poisoning (see below). The bed material consisted of a mixture of quartz sand and the respective CaO powders, i.e., 4.000 g of SiO<sub>2</sub> mixed with 0.125

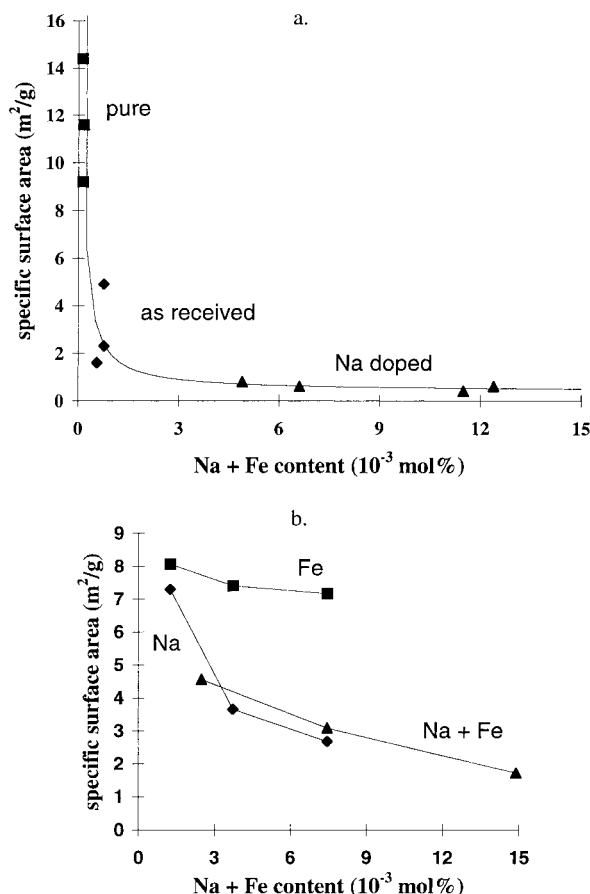


**Figure 1.** BET specific surface area (m<sup>2</sup>/g) as a function of impurity content for the investigated CaO materials listed in section A and in section B of Table 1.

g of CaO doped with Na and Na + Fe and 2.000 g of SiO<sub>2</sub> mixed with 0.063 g of Fe-doped CaO. Finally, the FTIR gas analyzer was replaced by a quadrupole mass spectrometer (Balzers, QMG 421) in order to measure the oxygen abstraction by CO. More details on this procedure and the experimental set up for surface oxygen abstraction can be found in previous work.<sup>11</sup>

The gases used were 5000 ppm NO, CO, CO<sub>2</sub>, and H<sub>2</sub> in Ar. The gases were mixed with pure Ar, and the flows were controlled using mass flow controllers (Brooks Type 5850E).

### III. Results

**III.1. Characterization of the Tested Materials.** In Table 1, the Fe and Na contents as well as the specific surface areas are listed for the investigated CaO powders. The Fe and Na contents in Table 1A were determined by atomic absorption spectroscopy, while in Table 1B the added concentrations are given. It is observed in Table 1A that the purification step, which was intended to lower the sodium content, also lowers the Fe content. The specific surface area of all investigated materials varies between 0.4 and 14.4 m<sup>2</sup>/g. In Figure 1, the specific surface area of the CaO powders is shown as a function of Na + Fe content. The results displayed in Figure 1a show a decrease in specific surface area with an increased Fe + Na content. It could be argued that this difference is not due to a difference in impurity content, but that different treatments of the respective powders influence the specific surface areas. This assumption can be excluded based on the results for the CaO material produced from calcium acetate, blank sample, which was treated in the same way as the Na-doped materials. A BET

surface area in the range of the pure materials, i.e., 11.6 m<sup>2</sup>/g, is obtained. In Figure 1b, it is shown that Fe impurities have a marginal effect on the specific surface area, while Na impurities affect it strongly. The trend for the latter is in agreement with the trend displayed in Figure 1a. Addition of equimolecular amounts of Fe and Na results in a pronounced decrease when a comparison is made based on the Na content alone.

**III.2. Catalytic Activity versus the Iron and Sodium Contents.** The decrease in specific surface area with increasing Na + Fe content has important consequences when evaluating the catalytic activities of these materials. To be able to evaluate the impurity effect on the catalytic activity, the reaction rate has to be formulated as a function of the surface area of the respective materials. This specific reaction rate is calculated from the material balance, assuming the order of reaction to be one for both NO and CO<sup>15,16</sup> and using the equimolecular consumption of NO and CO. The following relations are found:

$$r = (F/S)(1/y_{\text{NO}} - 1/y_{\text{NO}}^f)y_{\text{NO}}^2 \quad (1)$$

$$r = - (F/(S\alpha))(\ln(y_{\text{NO}}/y_{\text{NO}}^f) - \ln((\alpha + y_{\text{NO}})/(\alpha + y_{\text{NO}}^f)))y_{\text{NO}}y_{\text{CO}} \quad (2)$$

where  $F$  stands for the molecular flow,  $y$  for the molar ratio,  $r$  for the specific reaction rate,  $S$  for the surface area,  $\alpha$  for the difference in CO and NO feed, i.e.,  $y_{\text{CO}}^f - y_{\text{NO}}^f$ , and superscript  $f$  for the feed conditions. The former relation (1) gives the specific reaction rate for equimolecular feed mixtures, while the latter (2) is applicable for all other gas mixtures.

In Figure 2a, a dependency is observed of the specific reaction rate on the impurity content (Na + Fe) of the materials listed in Table 1A. This is seen for both CO and H<sub>2</sub> as reducing agents. It is shown that an impurity content increase correlates with an increased specific reaction rate for low impurity levels. For high impurity contents, such as for the materials promoted by sodium, the specific reaction rate is not that well-defined. This is mainly due to the uncertainty in the determination of the surface areas for these materials. Although both H<sub>2</sub> and CO behave similarly as reducing agents, some differences between them are observed for the Na-doped materials (Figure 2b). This will be shown to be due to CO<sub>2</sub> poisoning.

A relatively big spread in the specific reduction rates can be observed for the as-received materials. This is suggested to be due to the presence of other, unquantified impurities. To quantify the effect of Fe, new materials were prepared with controlled amounts of Na, Fe, and Na + Fe (Table 1B). In Figure 2c, the specific reaction rate for the NO reduction with H<sub>2</sub> at 800 °C is shown. An increasing specific reaction rate with increasing impurity content can be observed for all three groups of materials. Fe is seen to enhance the catalytic activity of CaO to a greater extent than Na when equimolecular amounts are compared. In the presence of low amounts of both Na and Fe, suppression of the catalytic activity is observed. An increased amount of impurities results in a decreased suppression as can be seen by the decreasing difference between the specific reaction rate of the (Na + Fe)-doped CaO and the specific reaction rates for the sum of the samples independently doped with Na and Fe.

**III.3. Measured Activation Energies for Heterogeneous NO Reduction.** The apparent activation energies for the NO reduction were determined with both CO and H<sub>2</sub> as reducing agents. Three of the previously described powders, listed in Table 1A, were investigated, i.e., one pure (calcined calcium

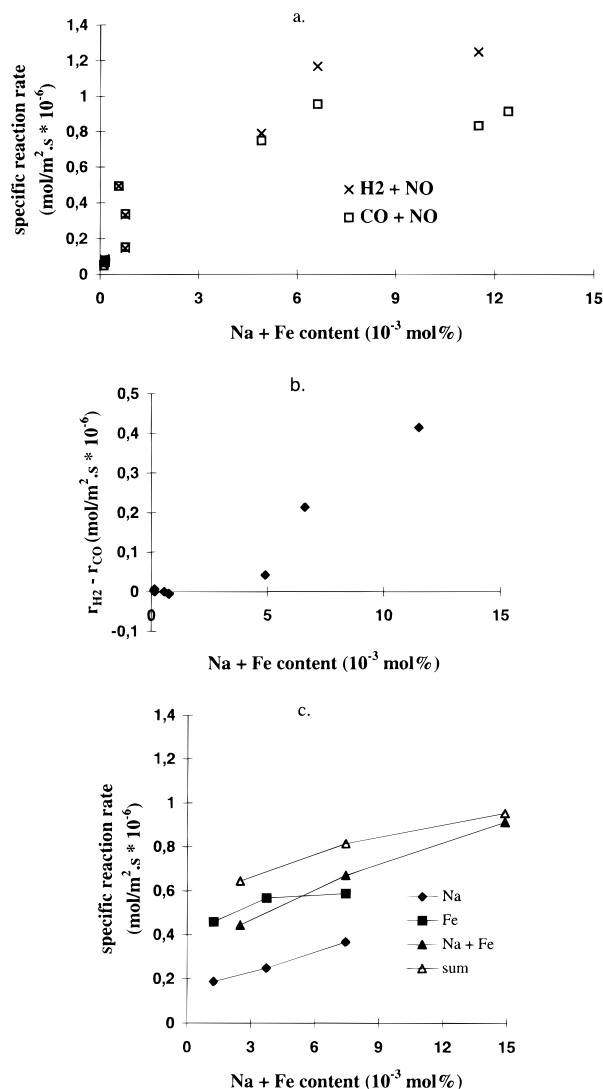
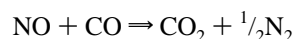


**Figure 2.** (a) Specific reaction rate for the reduction of NO with CO or H<sub>2</sub> as a function of Na + Fe content for the materials listed in Table 1A. (b) Difference in the specific reaction rate for CO and H<sub>2</sub> as reducing agents as a function of Na + Fe content for the materials listed in Table 1A. (c) Specific reaction rate for the reduction of NO with H<sub>2</sub> as a function of Na + Fe content for the materials listed in Table 1B.

acetate), one as-received (CaO, Fisher Scientific), and one Na-doped (label 1).

When investigating the mass balance, it was observed that NO and CO were consumed equimolarly and that the CO<sub>2</sub> production corresponded with the amounts of CO that had reacted. Based on these results, the following overall reaction is suggested for CO as the reducing species:



This discussion can be repeated for H<sub>2</sub> as the reducing agent producing H<sub>2</sub>O, since only negligible amounts of NH<sub>3</sub> were detected (<5%).

The reaction rates were evaluated, assuming the reaction to be first order in both NO and the respective reducing agent.<sup>15,16</sup> These assumptions lead to the following rate equation for the NO + CO reaction:

$$-d[\text{NO}]/dt = k[\text{NO}][\text{CO}] \quad (3)$$

Solving this differential equation, by applying a plug flow

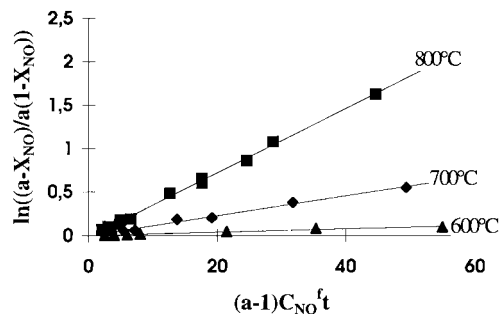


**Figure 3.** Absolute values of the  $\ln((\alpha - X_{\text{NO}})/(\alpha(1 - X_{\text{NO}})))$  versus  $(\alpha - 1)C_{\text{NO}}\tau$  for the NO + H<sub>2</sub> reaction over a CaO Fisher Scientific surface at 600, 700, and 800 °C.

reactor model, results in

$$\ln((\alpha - X_{\text{NO}})/(\alpha(1 - X_{\text{NO}}))) = k(\alpha - 1)C_{\text{NO}} \quad (4)$$

where  $\alpha$  is the ratio of the feed concentration of CO or H<sub>2</sub> to that of NO,  $X_{\text{NO}}$  is the fractional conversion of NO as defined earlier,  $C_{\text{NO}}\tau$  is the feed concentration of NO, and  $\tau$  is the residence time, defined as the ratio between the void volume of the bed and the volume flow rate.

When the absolute value of  $\ln((\alpha - X_{\text{NO}})/(\alpha(1 - X_{\text{NO}})))$  is plotted versus  $(\alpha - 1)C_{\text{NO}}\tau$ , the rate constant can be evaluated from the slope at a given temperature. This is shown in Figure 3 for the NO + H<sub>2</sub> reaction over the Fisher Scientific CaO surface at 600, 700, and 800 °C. A good correlation with the linear behavior is observed. This is consistent with the assumption concerning the reaction orders in NO and reducing agent. Similar curves were obtained for all materials at the investigated temperatures and for both reactions. Knowing the rate constants at the different temperatures, the Arrhenius equation

$$k = A \exp(-E_a/RT) \quad (5)$$

gives the apparent activation energies ( $E_a$ ) and the preexponential factors ( $A$ ) of the investigated reactions as slopes and  $Y$ -axis intercepts in  $\ln(k)$  versus  $1/T$  plots (Figure 4).

The measured apparent activation energies and the corresponding preexponential factors are given in Table 2. No significant differences in activation energies between the different materials are observed for the NO + H<sub>2</sub> reaction. Values between 26.1 and 26.6 kcal/mol are obtained. As opposed to this, significant differences are noticed using CO as the reducing agent. The spread in the apparent activation energies is much greater as values between 27.5 and 32.6 kcal/mol are obtained. This difference cannot be accounted for by experimental uncertainties. It was observed that an increase in  $E_a$  correlates with an increase in the preexponential factor. Such an effect has been reported in the literature for oxidative coupling of methane over similar materials,<sup>17,18</sup> where it was assigned to CO<sub>2</sub> poisoning. Korf et al. showed that CO<sub>2</sub> blocks the adsorption of the reactants, thereby lowering the activity and affecting the activation energy.<sup>19</sup> Also, apparent activation energies are calculated from rate constants at different temperatures, assuming identical surfaces. The results of the present study imply that, for the NO + CO reaction, the surfaces at the different temperatures are *not* identical. A decrease in temperature leads to an increase in CO<sub>2</sub> adsorption and thus an increased blocking of the active sites.

In Figure 5, the measured apparent activation energy for the NO + CO reaction is plotted versus the amounts of CO<sub>2</sub> per squared meter of surface in the outlet, taken at 800 °C.

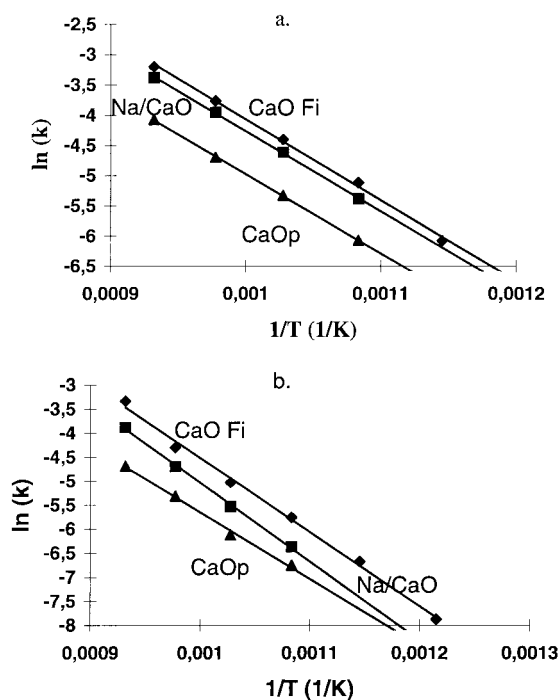


**Figure 4.** Arrhenius plots for the NO + H<sub>2</sub> (a) and NO + CO (b) reactions catalyzed by Na-doped CaO, pure CaO, and CaO Fisher Scientific.

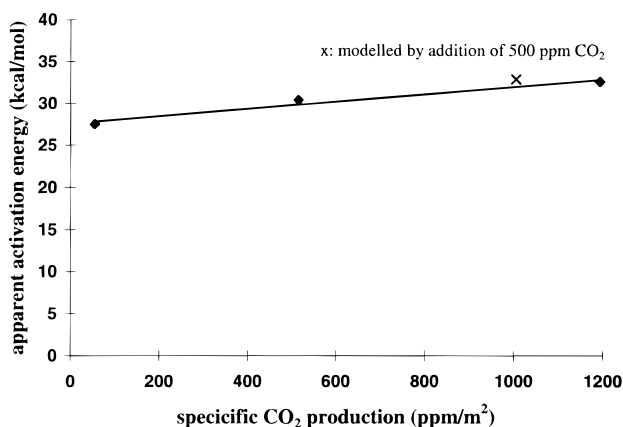


**Figure 5.** Relation between apparent activation energies for the NO + CO reaction and the specific CO<sub>2</sub> production for the different investigated materials. Included is also a modeled point obtained by adding 500 ppm CO<sub>2</sub> to the reaction mixture for the CaO (Fisher Scientific) powder.

Extrapolating the data to a CO<sub>2</sub> partial pressure of 0, results in an estimate of the true apparent activation energy for the NO + CO reaction of 27.6 kcal/mol. Support for such a treatment despite a CO<sub>2</sub> gradient along the reactor is found in Figure 5, where the apparent activation energy was determined when 500 ppm CO<sub>2</sub> was added to the feed reaction mixture for the Fisher Scientific CaO powder. A shift in the specific CO<sub>2</sub> production was modeled and seen to be consistent with the observed change in apparent activation energies for the different powders.

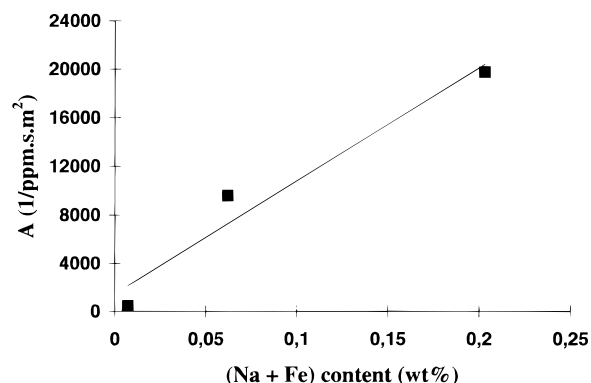


**Figure 6.** Specific preexponential factor (*A*: preexponential factor per surface area) versus the Na + Fe content of the investigated materials.

The corrected activation energy of 27.6 kcal/mol for the reduction of NO with CO is comparable with the 26.3 kcal/mol value for the NO + H<sub>2</sub> reaction where no CO<sub>2</sub> formation appears. The preexponential factors for the NO + CO reaction over all three materials can now be recalculated by constructing an Arrhenius plot based on the 800 °C results and the calculated apparent activation energy of 27.6 kcal/mol (excluding CO<sub>2</sub> poisoning). The corrected values are  $3.8 \times 10^3$ ,  $1.5 \times 10^4$ , and  $8.6 \times 10^3$  for CaO pure, CaO Fisher Scientific, and Na/CaO, respectively. These are in qualitative agreement with the preexponential factors for the NO + H<sub>2</sub> reaction shown in Table 2. The corrected values are systematically slightly higher than those for the NO + H<sub>2</sub> reaction and could be interpreted to still indicate some CO<sub>2</sub> poisoning at 800 °C. To make comparisons to the true preexponential factors, they have to be divided by the surface area. The preexponential factors related to the surface area are plotted versus the Na + Fe content in Figure 6 for each investigated material. The similarity between this figure and Figure 2a should be noted. In fact, this could be expected, since all three materials have similar activation energies, and therefore, the difference in NO reduction efficiency should be found in the preexponential factor.

**III.4. Surface Oxygen Abstraction and Reoxidation.** The *surface oxygen abstraction* of the materials listed in Table 1B is examined at 800 °C using CO as a probe molecule. The amount of CO<sub>2</sub> produced under CO exposure is a measure for the oxygen atoms that can be abstracted from the CaO surface, i.e., each CO<sub>2</sub> molecule stands for one abstracted oxygen. Typical CO<sub>2</sub> formation curves are shown in Figure 7 for the CaO powders promoted with Fe. Similar curves are obtained for the other tested materials, i.e., Na- and (Na + Fe)-doped CaO. A transient CO<sub>2</sub> production is observed of which the peak height and the peak width are correlated to the impurity content; i.e., an increase in impurity concentration results in an increased amount of formed CO<sub>2</sub>. The transient production is followed by a slowly decaying background due to a continuous reduction of the CaO matrix. In Figure 8, the integrated amounts of produced CO<sub>2</sub> under the first 700 s, i.e., the amounts of abstracted oxygens under this period, are shown as a function of the Na + Fe content. The amount of abstracted surface

**TABLE 2: Apparent Activation Energies for the NO + CO and NO + H<sub>2</sub> Reactions over the Different CaO Surfaces**

material	temp, °C	NO + CO			NO + H <sub>2</sub>		
		<i>E<sub>a</sub></i>	<i>A</i>	corr	<i>E<sub>a</sub></i>	<i>A</i>	corr
0.5 g CaO Fisher	550–850	30.4	$5.5 \times 10^4$	0.99	26.6	$1.1 \times 10^4$	0.99
0.5 g CaO pure	650–800	27.5	$3.7 \times 10^3$	0.99	26.1	$3.4 \times 10^3$	1
0.5 g Na/CaO	650–800	32.6	$8.6 \times 10^4$	1	26.3	$7.9 \times 10^3$	1
corrected		27.6			26.3		

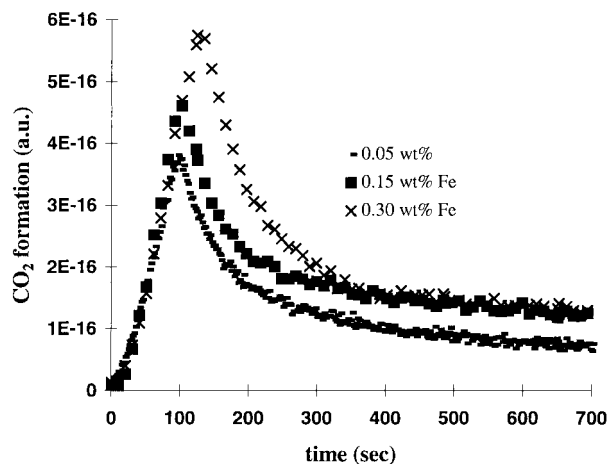


**Figure 7.** Transient  $\text{CO}_2$  production for the different Fe-doped CaO materials under CO exposure at 800 °C.

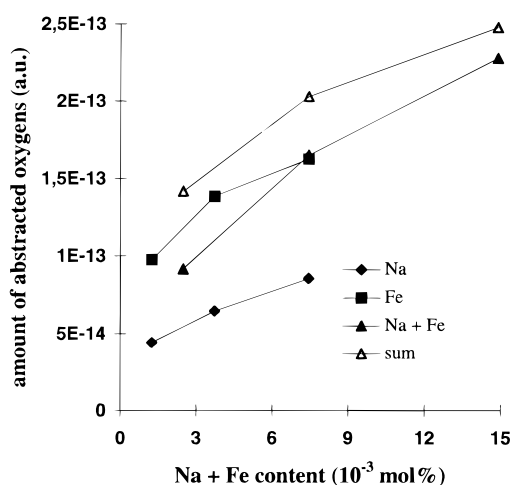


**Figure 8.** Amounts of abstracted oxygens during the first 700 s of CO exposure as a function of the Na + Fe content of the materials listed in Table 1B.

oxygens is observed to increase with impurity content for each group of materials. Comparing the oxygen abstraction for CaO powders promoted with Fe or Na, Fe impurities are seen to be more effective than equimolecular amounts of Na impurities.

Addition of both Na and Fe leads to a suppression of the oxygen abstraction. This is observed when the amount of abstracted oxygens for the (Na + Fe)-promoted materials is compared with the sum of the amounts for the separately promoted materials. This suppression is most pronounced for low impurity concentrations. Similar effects were observed for the specific reaction rate of the NO reduction with  $\text{H}_2$  at 800 °C. And indeed, combination of these two results, i.e., the amount of abstracted oxygens versus specific reaction rate, for all investigated materials listed in Table 1B results in a linear relation between the two as is shown in Figure 9. It is observed that an increase in the amount of abstracted oxygens results in an increased specific reaction rate. Extrapolation of this result to zero oxygen abstraction results in a very low specific reaction rate.

After exposure to CO, the materials were *reoxidized* by NO at 800 °C. During the NO exposure, a transient  $\text{N}_2$  formation was observed. The amounts of  $\text{N}_2$  formed were found to be about half the amounts of abstracted oxygens. This was expected from previous experiments<sup>11</sup> and is shown again in Figure 10.

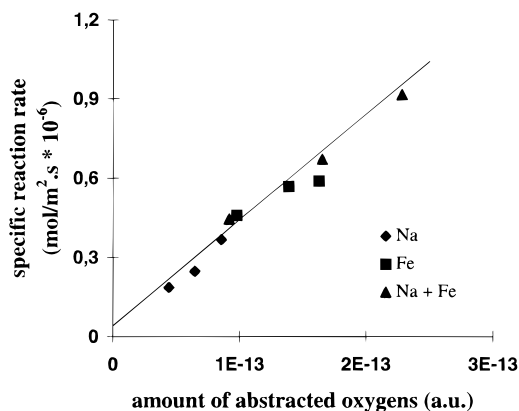


**Figure 9.** Specific reaction rate as a function of the amount of abstracted oxygens for the materials listed in Table 1B.

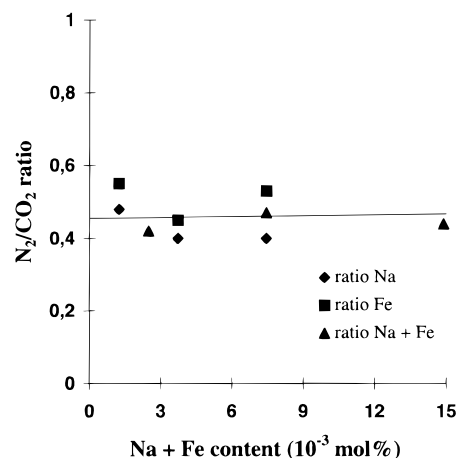
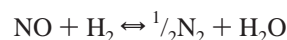
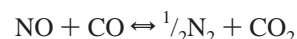


**Figure 10.** Ratio between the  $\text{N}_2$  formed during reoxidation by NO and the  $\text{CO}_2$  formed during CO exposure at 800 °C of the materials listed in Table 1B.

**III.5. Measured Activation Energies for Heterogeneous NO Reduction over MgO, SrO, and BaO.** The results so far indicate that the apparent activation energies for the two investigated reactions



are independent of the impurity content and of the reducing gas used,  $\text{H}_2$  or CO, if correction is made for the influence of  $\text{CO}_2$  poisoning for the latter. This independence can be used to determine the apparent activation energies of the other alkaline-earth oxides, i.e., MgO, SrO, and BaO. The MgO was provided by Fluka and had a maximum Na and Fe content of 0.2 and 0.005 wt %. The SrO (99.5% pure) and BaO (97% pure) were provided by Johnson Matthey. The trace metal content of the latter was specified to be less than 1%. The bed materials were pretreated in Ar at 900 °C for MgO and SrO and 1100 °C for BaO until neither  $\text{H}_2\text{O}$  nor  $\text{CO}_2$  desorption was observed. The obtained apparent activation energies for the reduction of NO by  $\text{H}_2$  are given in Table 3 and are seen to vary from 19.5 kcal/mol for MgO to 33.5 kcal/mol for BaO. The temperature intervals for determination of the activation energies (Table 3) were in all cases selected above the decomposition temperature of the respective hydroxides. In Figure 11, these values are plotted versus the respective lattice parameters and a correlation is observed.

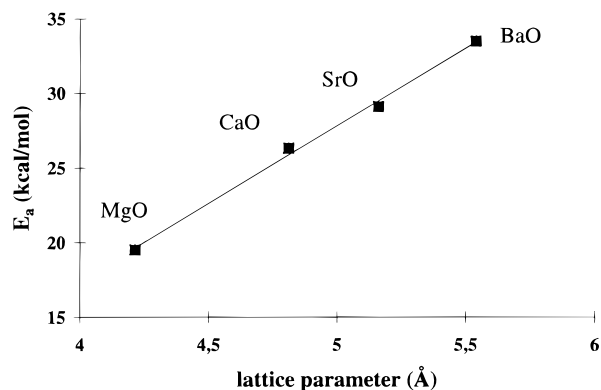


**Figure 11.** Apparent activation energy for the NO + H<sub>2</sub> reaction over alkaline-earth oxides as a function of the lattice parameter of these oxides.

**TABLE 3: Apparent Activation Energies for the NO + H<sub>2</sub> Reaction over Different Alkaline-Earth Metal Oxides**

material	temp. (°C)	E <sub>a</sub> , kcal/mol
MgO	650–850	19.5
CaO	650–800	26.3
SrO	750–850	29.1
BaO	900–1000	33.5

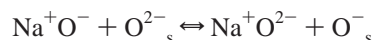
#### IV. Discussion

The presented results suggest that the rate-determining step for the examined reactions (shown above) is the same. Temperature-programmed reduction experiments have shown that the activation energy for the surface-oxygen-abstraction step with CO is about 25 kcal/mol,<sup>11</sup> while the apparent activation energy for the breaking of an NO bond is lower than 10 kcal/mol.<sup>11</sup> The former value, 25 kcal/mol, is similar to the apparent activation energies measured here. Based on these results, it is suggested that the rate-determining step can be ascribed to the picking out of surface oxygens, leaving the electrons of the removed oxygen ion in the substrate.

In Figures 2a and 6, the influence of the trace metal impurities on the catalytic activity of CaO is shown for the materials listed in Table 1A. Although these materials were only analyzed for the sodium and iron contents, it is believed that the results will not change if other impurities present in the materials would be included in the analysis. In fact, a further improved correlation between impurity content and specific reaction rate for the NO reduction is expected. The trace metal impurities can be separated into two main groups: metals having only one oxidation state and metals appearing in several oxidation states. The alkali metals and the alkaline-earth metals belong to the former group, while the transition metals belong to the latter. In the first group, a distinction should be made between the alkali metals, with oxidation state +I, and the alkaline-earth metals, oxidation state +II. Substituting a Ca<sup>2+</sup> ion with a Na<sup>+</sup> leads to an electrostatically unbalanced situation in the CaO matrix. This can be neutralized by the formation of O<sup>-</sup> species and/or oxygen vacancies in the crystal structure. The formation of O<sup>-</sup> species has been shown by electron paramagnetic resonance for a number of alkaline-earth systems doped with alkali metals: e.g., Li-doped MgO and Li- and Na-doped CaO.<sup>9,10,20–24</sup> The amount of alkali-metal ions that can be kept in solid solution in an alkaline-earth metal oxide matrix is limited. From the moment the solid solubility is exceeded, a Na-rich second phase will form. The sodium ions in this second phase will not lead to the formation of O<sup>-</sup> species and will have different catalytic properties toward the investigated reactions. This is suggested to be observed in Figure 2 for Na

+ Fe concentrations exceeding about 0.3 wt % and is in line with the discussion put forward by Schoderböck and Lahaye for Fe impurities in quartz sand.<sup>14</sup>

The role of O<sup>-</sup> species in the catalytic activity of Li-doped MgO and Na-doped CaO substrates toward the oxidative coupling of methane has been discussed extensively. These materials display high selectivity toward this reaction.<sup>25</sup> Although the reaction mechanism is not fully understood, a redox mechanism involving O<sup>-</sup> species introduced by substitution of Mg or Ca by Li or Na has been suggested. The surface O<sup>-</sup> species can abstract a hydrogen atom and produce an alkyl radical from methane. The subsequent dehydroxylation of the surface leads to an inactive surface for further alkyl formation. The surface is regenerated by exposure to oxygen. This reaction mechanism was proposed by Lin et al.,<sup>10</sup> and it illustrates clearly the role of the O<sup>-</sup> species in the catalytic activity of these types of materials. The electric conductivity of pure MgO, known to be an insulator, is enhanced by a factor of 10<sup>4</sup> by promotion with lithium ions.<sup>26</sup> Lin et al. referred to this result when suggesting that defects in the bulk could also contribute to the catalytic activity by a hole transport mechanism exploiting O<sup>-</sup> species in the bulk:



Examination of the same reaction over ultrathin films of MgO and Li-doped MgO and characterization of the respective films by high-resolution electron energy loss spectroscopy lead Wu et al. to a different conclusion.<sup>9</sup> These authors suggested that [Li<sup>+</sup>O<sup>-</sup>] defects promote the production of F centers in the vicinity of the surface.

It is not clear how transition-metal ions are incorporated in the structure, whether in solid solution or in a second phase, or even in which oxidation state they appear. However, the stability of a certain oxidation state will depend on, e.g., temperature, gas atmosphere, and other impurities present. Promotion of an oxide matrix with transition-metal ions has been addressed by Cimino.<sup>27</sup> It was concluded that when the guest ion has the same valence and is of similar size as the host ion and the matrix offers sites of symmetry, compatible with the electronic structure of the guest ion, then a true solid solution can be formed. However, when the guest ion has a different charge than the host ion, a solid solution will be obtained only if its extra charge is compensated, e.g., Cr<sup>3+</sup> by Li<sup>+</sup> in MgO. This is in agreement with electron paramagnetic resonance (EPR) experiments for unstable [Li<sup>+</sup>O<sup>-</sup>] defects in doped MgO.<sup>28</sup> In Fe-containing samples, it was observed that unstable [Li<sup>+</sup>O<sup>-</sup>] defects, created by  $\gamma$  irradiation at 77 K, disappear at temperatures as low as 200 K, while simultaneously the Fe<sup>3+</sup> concentration increased. For the materials investigated here, this understanding would imply that the highest oxidation state for the respective transition-metal impurity is the most likely, probably compensated by Na<sup>+</sup> ions in its vicinity. However, it has been shown by several authors that the addition of a transition metal to alkali-metal-promoted alkaline-earth oxide materials can give rise to significant improvements in catalytic behavior toward the oxidative coupling of methane.<sup>29–32</sup> Promotion of the CaO by transition-metal addition was observed in the present study for the reduction of NO with H<sub>2</sub>. However, simultaneous addition of equimolecular amounts of Na and Fe was found to suppress the specific catalytic activity when comparing to the sum of the reaction rates obtained for the impurities added separately (Figure 2c). This is consistent with the EPR results as discussed in ref 28, as an electrostatically balanced situation based on Na<sup>+</sup> and Fe<sup>3+</sup> ions is understood

to form. In such a scenario, the addition of Na does not lead to the formation of  $O^-$  species, and consequently, only Fe impurities can participate in the redox process. The results displayed in Figure 2c show further that addition of Fe is more effective than addition of equimolecular amounts of Na. A possible explanation would be the formation of oxygen vacancies which compete with  $O^-$  production in the case of Na addition to maintain an electrostatically balanced situation. Oxygen vacancies are not expected to form in the bulk for only Fe addition. The role of Fe impurities on the catalytic activity of CaO has not been addressed in the literature. A mechanism based on a reduction and reoxidation of the surface is demonstrated by an oxygen-abstraction step under CO exposure (Figure 7) and a subsequent  $N_2$  formation under NO exposure (Figure 11).

While details can be discussed, the main result of this work is to demonstrate the extent to which impurity content correlates with the catalytic activity (Figure 2a and -c) and with the amount of abstracted oxygens (Figure 8). Combining these observations demonstrates that a decrease in the amount of abstracted oxygen from the substrate corresponds with a decreased specific reaction rate (Figure 9). This demonstrates a definite relation between the impurity content, the amount of abstracted oxygens, and the specific reaction rates.

Similar understandings as produced for CaO are suggested to also hold for the MgO, SrO, and BaO substrates. The linear dependence between the apparent activation energy of the NO reduction on the lattice parameter for these materials can be interpreted to support both the semiconductor model and the model based on stabilization of F centers.

## V. Conclusion

Correlation between the impurity content and the specific reaction rate of the different types of CaO materials toward the NO reduction with CO and  $H_2$  was demonstrated. The apparent activation energy for the overall  $NO + H_2$  reaction was determined to about 26.5 kcal/mol. A similar value, 27.5 kcal/mol, was found for the  $NO + CO$  reaction after correction for  $CO_2$  poisoning. Both reactions have previously been suggested to comprise (i) a surface-oxygen-abstraction step and (ii) a reoxidation step. The former one has been pointed out as the rate-determining step.

The presence of impurities in the CaO crystal structure was shown to have no significant influence on the apparent activation energy. The effect of increasing the impurity level results in a proportional increase in the number of active sites as was observed by an increase in the specific preexponential factor, specific reaction rate, and amount of abstracted oxygens. The other alkaline-earth oxides were also shown to be catalytically active for the NO reduction, and the apparent activation energy for the  $NO + H_2$  reaction was shown to correlate linearly with the lattice parameter. Our results emphasize the importance of  $O^-$  sites, created by the  $Na^+$  impurities. Such electron sinks

have previously been suggested to play a vital role in the surface reaction mechanism. The precise function, whether localized electron sinks or contributing to an  $O^-$  impurity band in a semiconductor model, could not be resolved. The role of Fe, shown to be more effective than equimolecular amounts of Na, is not fully understood. However, a redox mechanism based on  $Fe^{2+}/Fe^{3+}$  cannot be excluded.

**Acknowledgment.** We are in debt to the Swedish National Board for Industrial and Technical Development for financial support (NUTEK).

## References and Notes

- Zhdanov, V. P.; Kasemo, B. *Surf. Sci. Rep.* **1997**, *29*, 31.
- Wong, K.; Johansson, S.; Kasemo, B. *Faraday Discuss.* **1996**, *105*.
- Goodman, D. W.; Peden, C. H. F. *J. Phys. Chem.* **1986**, *92*, 4839.
- Berlowitz, P. J.; Peden, C. H. F.; Goodman, D. W. *J. Phys. Chem.*, **1988**, *90*, 5213.
- Hamada, H. *Catal. Today* **1994**, *22*, 21.
- Chu, W. F.; Rohr, F. J. *Solid State Ionics* **1988**, *28-30*, 1540.
- Voorhoeve, F. J. H.; Remeika, J. P.; Freeland, P. E.; Matthias, B. T. *Science* **1972**, *177*, 353.
- Voorhoeve, F. J. H.; Remeika, J. P.; Trimble, L. E. *Ann. N. Y. Acad. Sci.* **1976**, *272*, 3.
- Wu, M.-C.; Truong, C. M.; Coulter, K.; Goodman, D. W. *J. Catal.* **1993**, *140*, 344.
- Lin, C.-H.; Wang, J.-X.; Lunsford, J. H. *J. Catal.* **1988**, *111*, 302.
- Acke, F.; Panas, I.; Strömberg, D. *J. Phys. Chem. B* **1997**, *101*, 6484.
- Henrich, V. E. *Rep. Prog. Phys.* **1985**, *48*, 1481.
- Zhang, X.; Walters, A. B.; Vannice, M. A. *J. Catal.* **1994**, *146*, 568.
- Schoderböck, P.; Lahaye, J. *Appl. Surf. Sci.* **1996**, *93*, 109.
- Tsujumura, M.; Furusawa, T.; Kunii, D. *J. Chem. Eng. Jpn* **1983**, *16*, 132.
- Tsujumura, M.; Furusawa, T.; Kunii, D. *J. Chem. Eng. Jpn*, **1983**, *16*, 524.
- Coulter, K.; Goodman, D. W. *Catal. Lett.*, **1993**, *20*, 169.
- Xu, M.; Shi, C.; Yang, X.; Rosynek, M. P.; Lunsford, J. H. *J. Phys. Chem.* **1992**, *96*, 6395.
- Korf, S. J.; Roos, J. A.; de Bruijn, N. A.; Van Ommen, J. G.; Ross, J. R. H. *J. Chem. Soc., Chem. Commun.* **1987**, 1433.
- Tohver, H. T.; Henderson, B.; Chen, Y.; Abraham, M. M. *Phys. Rev. B* **1972**, *5*, 3276.
- Chen, Y.; Tohver, H. T.; Narayan, J.; Abraham, M. M. *Phys. Rev. B* **1977**, *16*, 5535.
- Olson, D. N.; Orera, V. M.; Chen, Y.; Abraham, M. M. *Phys. Rev. B* **1980**, *21*, 1258.
- Wang, J.-X.; Lunsford, J. H. *J. Phys. Chem.* **1986**, *90*, 5883.
- Lin, C.-H.; Ito, T.; Wang, J.-X.; Lunsford, J. H. *J. Am. Chem. Soc.* **1987**, *109*, 4808.
- Ito, T.; Lunsford, J. H. *Nature*, **1985**, *314*, 721.
- Chen, Y.; Kernohan, R. H.; Boldú, J. L.; Abraham, M. M. *Solid State Commun.* **1980**, *33*, 441.
- Cimino, A. *Chim Ind* **1974**, *56*, 27.
- Boldú, J. L.; Abraham, M. M.; Chen, Y. *Phys. Rev. B*, **1979**, *19*, 4421.
- Larkins, F. P.; Nordin, M. R. In *Methane Conversion*; Bibby, D. M., Chang, C. D., Howe, R. F., Yurchak, S., Eds.; Elsevier: Amsterdam, 1988; p 409.
- Bi, Y.; Zhen, K.; Jiang, Y.; Teng, C.; Yang, X. *Appl. Catal.* **1988**, *39*, 185.
- Bartsch, S.; Falkowski, J.; Hofmann, H. *Catal. Today* **1989**, *4*, 421.
- Korf, S. J.; McNamara, D.; van Ommen, J. G.; Ross, J. R. H. *Appl. Catal.* **1989**, *56*, 119.